

SceneTracker: Long-term Scene Flow Estimation Network

Bo Wang, Jian Li, Yang Yu, Li Liu, Zhenping Sun, Dewen Hu

Abstract—Considering the complementarity of scene flow estimation in the spatial domain’s focusing capability and 3D object tracking in the temporal domain’s coherence, this study aims to address a comprehensive new task that can simultaneously capture fine-grained and long-term 3D motion in an online manner: long-term scene flow estimation (LSFE). We introduce SceneTracker, a novel learning-based LSFE network that adopts an iterative approach to approximate the optimal trajectory. Besides, it dynamically indexes and constructs appearance and depth correlation features simultaneously and employs the Transformer to explore and utilize long-range connections within and between trajectories. With detailed experiments, SceneTracker shows superior capabilities in handling 3D spatial occlusion and depth noise interference, highly tailored to the LSFE task’s needs. Finally, we build the first real-world evaluation dataset, LSFDriving, further substantiating SceneTracker’s commendable generalization capacity. The code and data for SceneTracker is available at <https://github.com/wsource/SceneTracker>.

Index Terms—Long-term Scene Flow Estimation, Scene Flow Estimation, 3D Object Tracking, Transformer



INTRODUCTION

The precise and online capture and analysis of fine-grained long-term 3D object motion play a pivotal role in scene comprehension. By accurately capturing the 3D movement of objects, detailed data on position, velocity, acceleration, and more can be obtained, allowing for an in-depth understanding of how objects move and interact within specific environments. This information holds critical significance across various domains, including robotics, autonomous driving, and virtual reality.

The existing work primarily focuses on scene flow estimation (SFE) and 3D object tracking (3D OT) tasks, which partially address the issue of online 3D motion capture. SFE aims to estimate the pixel-wise/point-wise 3D motion between consecutive stereo, RGB-D, or point cloud data, and it can capture fine-grained instantaneous 3D displacement. However, SFE is unable to capture the 3D trajectory over a period of time robustly. Due to the presence of occlusions, per-frame 3D displacements cannot form the trajectory through simple chaining. 3D OT aims to achieve long-term tracking of targets and employs a 3D bounding box to mark the position and size of the target at each moment. It operates on the object level, requires prior modeling of the object [1, 2, 3], and provides limited information about 3D deformations within the object.

Considering the complementarity of SFE in the spatial domain’s focusing capability and 3D OT in the temporal domain’s coherence, this study aims to address a comprehensive new task that can simultaneously capture fine-grained and long-term 3D motion: long-term scene flow estimation (LSFE). LSFE seeks to estimate the query pixel/point’s 3D trajectory within a continuous stereo, RGB-D, or point cloud sequence online. Our task can be seen as an extension of SFE into a broader temporal domain or an extension of 3D OT into the pixel/point-level spatial domain.

We propose SceneTracker, the first LSFE method, which takes a T -frame RGB-D video and the camera intrinsics as input, along with the starting 3D coordinates x, y, z and starting time t of an arbitrary 3D target to track, and produces a $T \times 3$ matrix as output, representing the positions in the camera coordinate system of the target across the given frames. SceneTracker adopts an iterative approach to approximate the optimal trajectory, overcoming the significant displacement challenges between frames. Besides, it dynamically indexes and constructs appearance and depth correlation features simultaneously, enhancing the ability to localize the target 3D position. Finally, it employs the Transformer to explore and utilize long-range connections within and between trajectories, further improving the accuracy of LSFE.

We train and evaluate the proposed method on the large-scale synthetic dataset. Compared to the scene flow-based chaining method and tracking any point-based depth indexing method, the proposed SceneTracker is highly tailored to the needs of the LSFE task. It can effectively address 3D spatial occlusion and depth noise interference, achieving median 3D error reductions of 57.7% and 86.6%, respectively.

Moreover, we build a real-world evaluation dataset, LSF-Driving. This dataset is geared towards the autonomous driving realm, providing 3D trajectory annotations for points on objects with diverse motion attributes and rigidities. Specifically, the tracked points are sampled from static backgrounds, moving rigid vehicles, and moving non-rigid pedestrians. Addressing the complexity of local non-linear motion in pedestrian joints and garments, we build a semi-automated annotation pipeline capable of efficiently and accurately annotating 3D trajectories.

The study offers the following contributions:

- To better capture the fine-grained and long-term 3D motion, a comprehensive new task, long-term scene flow estimation, is studied.
- A novel learning-based LSFE network, SceneTracker, is presented. SceneTracker shows superior capabilities in handling 3D spatial occlusion and depth noise interference.
- We build the first real-world evaluation dataset, LSFDriving, further substantiating SceneTracker’s commendable generalization capacity.

Bo Wang, Jian Li, Yang Yu, Zhenping Sun, and Dewen Hu are with the College of Intelligence Science and Technology, National University of Defense Technology, Changsha, China.

Li Liu is with the College of Electronic Science and Technology, National University of Defense Technology, Changsha, China.

Bo Wang and Jian Li contributed equally to this work. Corresponding authors: Zhenping Sun (sunzhenping@nudt.edu.cn) and Dewen Hu (dwhu@nudt.edu.cn).

arXiv:2403.19924v3 [cs.CV] 6 May 2024

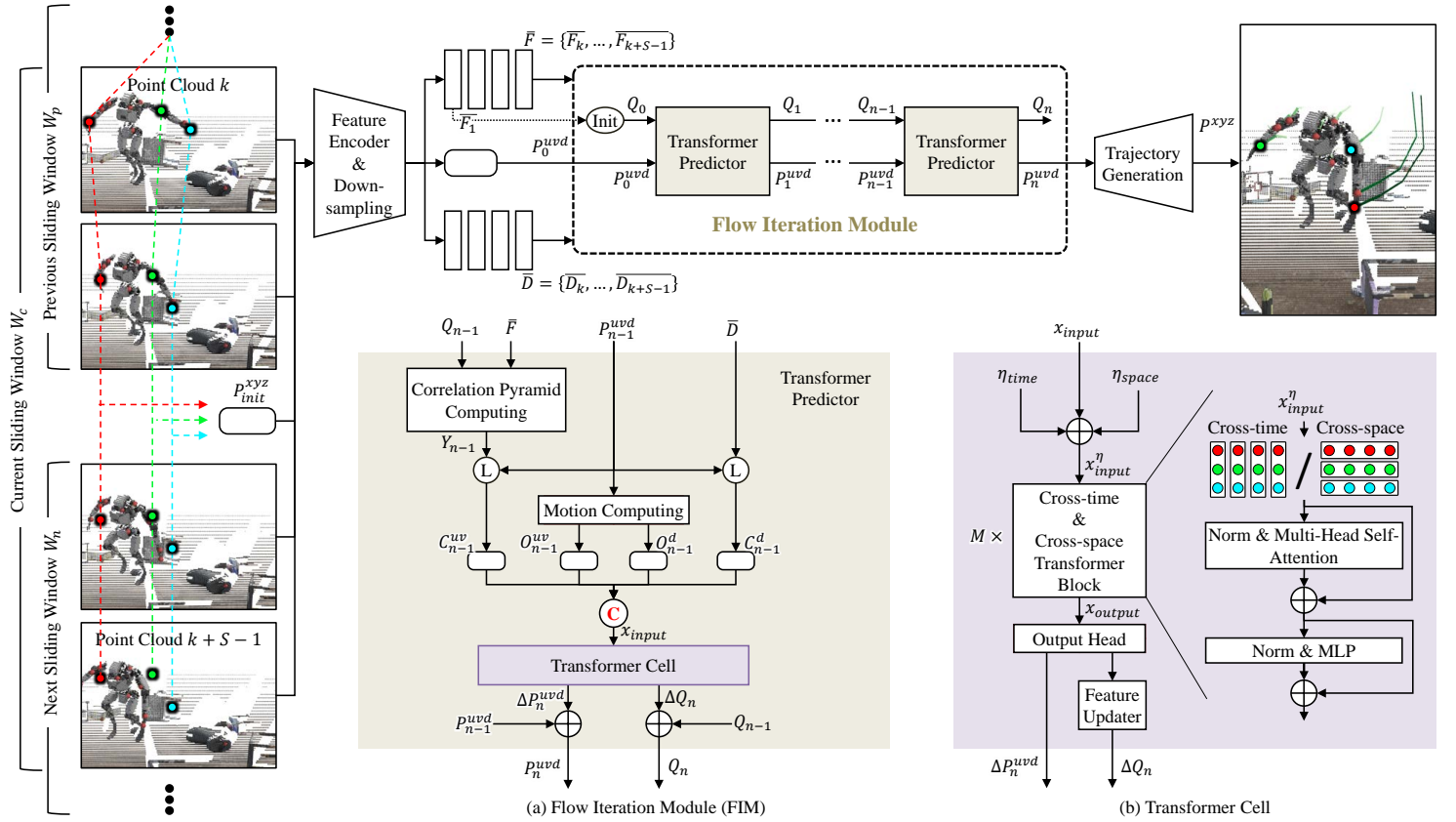


Fig. 1: The overall architecture of the proposed SceneTracker. We use \mathbf{C} to represent a concatenation operation. The detailed data flow for iteratively updating the 3D trajectory is summarized as a Flow Iteration Module (FIM) in the brown part.

2 RELATED WORKS

2.1 Scene Flow Estimation

The existing methods generally rely on feature similarities as their underlying principle. FlowNet3D [4] operates directly on point clouds with PointNet++ [5]. CamLiFlow [6] refines the optical flow and scene flow from the two frames’ feature similarity tensor in a coarse-to-fine way with two branches. OpticalExp [7] uses optical expansion to recover the pixel’s motion in depth between frames. It can estimate the final depth value of the second frame by combining the first frame’s depth, indirectly estimating the scene flow per pixel. The existence of occlusion issues severely constrains the accuracy of SFE. To tackle the occlusion problem, RAFT-3D [8] and RigidMask [9] focus on introducing rigid motion priors explicitly and implicitly, respectively.

2.2 Tracking Any Point

Unlike optical flow estimation methods [10, 11, 12, 13, 14, 15, 16], which focuses on local instantaneous motion, the tracking any point (TAP) task focuses more on the global motion trajectory in the image domain. TAP-Net [17] computes cost volumes for the first frame and every intermediate frame of the video independently, which will be directly used for regression of position and occlusion status. MFT [18] performs the chaining of optical flow and occlusion status by estimating the uncertainty. Cotracker [19] utilizes the strong correlation between multiple tracking points for joint tracking. PIPs++ [20] introduces 1D convolution and dynamic templates, improving the tracking survival rate over longer time spans in comparison to its previous version [21]. In contrast to the TAP task, LSFE involves overcoming

inherent noise in depth data and considering the 3D structure of objects and their motion patterns to track trajectories in 3D space accurately.

2.3 Reconstruction-based Offline Methods

Inspired by 3D-GS [22], which is notable for its pure explicit representation and differential point-based splatting method, many works have started to use 3D Gaussian to reconstruct dynamic scenes and render novel views. Dynamic 3D Gaussians [23] models dynamic scenes by tracking the position and variance of each 3D Gaussian at each timestamp. 4D-GS [24] proposes 4D Gaussian Splatting as a holistic representation for dynamic scenes rather than applying 3D-GS for each frame. After training on the complete multi-view videos, these methods calculate 3D trajectories based on the Gaussian deformations. In contrast to this offline approach, the LSFE task focuses more on challenging scenarios involving constrained observations, limited response time, and future uncertainty.

3 PROPOSED METHOD

3.1 Overall Architecture of SceneTracker

Our goal is to track 3D points throughout a 3D video. We formalize the problem as follows. A 3D video is a sequence of T RGB frames $\bar{I}_t \in \mathbb{R}^{3 \times H \times W}$ along with their depth maps. Estimating the long-term scene flow amounts to producing the 3D trajectories $P^{xyz} \in \mathbb{R}^{N \times T \times 3}$ in the camera coordinate system for N query points with known initial positions. By default, all tracking starts from the first frame of the video. It is worth noting

that our method can flexibly start tracking from any frame. The overall architecture of our method is shown in Fig. 1.

Trajectory initialization The first step of the initialization is to divide the entire video into several sliding windows. We partition it with a window size of S and a sliding step of $S/2$. As shown on the left side of Fig. 1, we need to track N query points, taking the red, green, and blue points as examples.

For the first sliding window, the positions are initialized as the initial positions of the query points. For the other sliding windows, the first $S/2$ frames are initialized based on the estimated results of the last $S/2$ frames of the previous sliding window, and the last $S/2$ frames are all initialized based on the estimated result of the last frame of the previous sliding window. Now, taking any current sliding window W_c as an example, we can obtain the initialized trajectories $P_{init}^{xyz} \in \mathbb{R}^{N \times T \times 3}$.

Feature Encoder and downsampling Our network is performing inference at resolution $\frac{H}{s} \times \frac{W}{s}$. Here, $s = 8$ is a downsampling factor utilized for efficiency. First, we use a Feature Encoder network to extract image features $\bar{F} = \{\bar{F}_k, \dots, \bar{F}_{k+S-1}\}$ from $\{I_k, \dots, I_{k+S-1}\}$ in the current sliding window W_c , assuming that W_c 's first frame is the entire video's k th frame. The Feature Encoder is a convolutional neural network comprising 8 residual blocks and 5 downsampling layers.

Unlike processing RGB images, we directly take equidistant samples at intervals of s from the S -frame original depth maps, thereby obtaining the depth maps $\bar{D} = \{\bar{D}_k, \dots, \bar{D}_{k+S-1}\}$ at $1/s$ of the original resolution. In addition, we transform P_{init}^{xyz} from the camera coordinate system to a uvd coordinate system composed of the uv plane and the depth dimension with the camera intrinsics $K = (f_x, f_y, c_x, c_y)$, resulting in P_{init}^{uvd} . The mathematical expressions of the conversion are as follows,

$$P_{init}^{uvd} = \begin{bmatrix} P_{init}^u \\ P_{init}^v \\ P_{init}^d \end{bmatrix} = \begin{bmatrix} f_x \cdot P_{init}^x / P_{init}^z + c_x \\ f_y \cdot P_{init}^y / P_{init}^z + c_y \\ P_{init}^z \end{bmatrix}. \quad (1)$$

To match the generated \bar{F} and \bar{D} , we downsample the initialized trajectory to generate the P_0^{uvd} .

Updates of template feature and trajectory In the Flow Iteration Module, we iteratively update the query points' template features and 3D trajectories. When processing the first sliding window's first frame, we perform bilinear sampling on \bar{F}_1 using the uv coordinates of the query points to obtain \bar{F}_1 's initial template feature. Then, we replicate this feature S times along the temporal dimension to obtain the initial template feature Q_0 for all subsequent sliding windows. Each sliding window will have a consistent Q_0 and different P_0^{uvd} . After n iterations of the same Transformer Predictor module, they will be updated to Q_n and P_n^{uvd} .

Trajectory output We first upsample P_n^{uvd} to generate P^{uvd} to match the original input resolution. Then, we combine the camera intrinsics K to transform P^{uvd} from the uvd coordinate system to the camera coordinate system, resulting in P^{xyz} . Finally, we chain all P^{xyz} estimated from the sliding windows. The overlapping parts between adjacent windows take the results from the latter window.

3.2 Flow Iteration Module

Like optical and scene flow, LSFE also faces the significant challenge of large inter-frame displacements. We draw on RAFT [14] and CoTracker [19], using an iterative approach to approximate the optimal result. At the same time, we use Transformer to model long-range dependencies within and between N 3D

trajectories of length S . Finally, from a 2D perspective, we synchronize the extraction of the apparent and depth correlation features, which unifies the originally fragmented image uv and depth dimensions. Based on the above considerations, we design the Flow Iteration Module (FIM) for updating the template feature Q_0 and trajectory P_0^{uvd} , as shown in Fig. 1 (a).

Taking the FIM's n th iteration as an example, the Transformer Predictor network requires to use Q_{n-1} , \bar{F} , P_{n-1}^{uvd} , and \bar{D} to construct the input for a Transformer Cell, which involves concatenating the apparent correlation feature C_{n-1}^{uv} , the depth correlation feature C_{n-1}^d , the apparent motion O_{n-1}^{uv} , and the depth motion O_{n-1}^d . The Transformer Cell outputs residuals, ΔQ_n and ΔP_n^{uvd} , to update Q_{n-1} and P_{n-1}^{uvd} to Q_n and P_n^{uvd} , serving as the output for the current iteration.

Apparent correlation feature Before constructing the apparent correlation feature C_{n-1}^{uv} , a l -layer correlation pyramid Y_{n-1} between Q_{n-1} and \bar{F} is calculated by taking the dot product between all pairs of feature vectors at the same frame time and pooling the last two dimensions. Then, the network uses P_{n-1}^{uvd} to lookup Y_{n-1} to obtain C_{n-1}^{uv} . Specifically, C_{n-1}^{uv} is obtained through bilinear sampling of Y_{n-1} layer by layer with the grid size $(2 \times r + 1)^2$ and then concatenating. Here, r is the local neighborhood radius.

Depth correlation feature The network uses P_{n-1}^{uvd} to lookup \bar{D} to obtain C_{n-1}^d . Specifically, C_{n-1}^d is obtained through bilinear sampling of \bar{D} 's inverse depth map and calculating the residual with the depth prediction P_{n-1}^d 's inverse.

Apparent and depth motion We obtain the apparent motion O_{n-1}^{uv} and the depth motion O_{n-1}^d by calculating the differences in uv positions and depths between each frame and the first frame ($t = k$) of the current window W_c :

$$O_{n-1}^{uv} = [P_{n-1}^{uv} - P_{n-1,k}^{uv}, \eta(P_{n-1}^{uv} - P_{n-1,k}^{uv})] \quad (2)$$

$$O_{n-1}^d = P_{n-1}^d - P_{n-1,k}^d \quad (3)$$

$$(4)$$

Here $\eta(\cdot)$ is the sinusoidal position encoding.

3.3 Transformer Cell Network

In the Transformer Cell network, we perform feature extraction and enhancement on the concatenated input feature x_{input} and then predict the residuals ΔP_n^{uvd} and ΔQ_n , as shown in Fig. 1 (b).

First, x_{input} will be sinusoidally encoded separately in temporal and spatial dimensions to obtain η_{time} and η_{space} . Then, we perform element-wise addition on x_{input} , η_{time} , and η_{space} to obtain x_{input}^η . Afterward, x_{input}^η will undergo $2 \times M$ Transformer Blocks for feature enhancement, with Cross-time and Cross-space Transformer Blocks being executed alternately. The two types of Transformer Blocks divide x_{input}^η into tokens based on time points and trajectories, respectively. After tokenization, both types of Transformer Blocks will sequentially undergo a normalization layer, multi-head self-attention layer, normalization layer, and MLP layer, accompanied by two skip connections. The model can effectively explore and utilize long-range connections within and between trajectories through the operations above.

The final Transformer Block outputs x_{output} , which is then fed into an Output Head network. The Output Head network comprises a fully connected layer, and its output can be split into ΔP_n^{uvd} and an intermediate feature. The intermediate feature will be input into a Feature Updater network, consisting of a normalization layer, a fully connected layer, and a GELU activation layer. The Feature Updater network outputs ΔQ_n .



Fig. 2: Example of producing LSFE annotations for pedestrian samples. We combine the left image and depth map sequence to form the RGB-D video. Once the left video’s 2D trajectory and disparity sequence are determined, we can utilize the binocular camera’s calibration parameters to convert them into the ground truth 3D trajectory.

3.4 Training and Inference

Our method for training involves using a T -frame 3D video as a data unit and the query points’ 3D trajectories to supervise the network’s outputs.

We supervise our network in an unrolled fashion to properly handle semi-overlapping sliding windows. L_{3D} is used to measure the error of trajectory prediction. Given the ground truth uv position P_{GT}^{uv} and depth P_{GT}^d for any sliding window, we define the loss as follows (for simplicity, we omit the indices of the windows):

$$L = L_{3D} = \sum_{W=W_1}^{W_{max}} \sum_{i=1}^n \gamma^{n-i} \cdot (\|P_i^{uv} - P_{GT}^{uv}\|_1 + \alpha \cdot \left\| \frac{1}{P_i^d} - \frac{1}{P_{GT}^d} \right\|_1) \quad (5)$$

Here we set $\gamma = 0.8$ and $\alpha = 250$. W_{max} is the final sliding window.

4 PROPOSED DATASET

Generally, sparse annotations are only available for rigid bodies across adjacent frames in real-world datasets [25, 26] of SFE. Differing from these datasets, the proposed LSFE dataset requires additional annotations of trajectories that span across multiple frames and are not limited to rigid bodies. Given a temporal segment of autonomous driving data, we aim to construct a T -frame RGB-D video and the 3D trajectory of interested points in the first frame. Specifically, the interested points are sampled from static backgrounds, moving rigid vehicles, and moving non-rigid pedestrians.

4.1 Annotations on Backgrounds

First, we utilize the camera’s intrinsic and extrinsic parameters to extract the first frame’s LiDAR points, which can be projected correctly into the image. Then, we use the bounding boxes from 2D object detection to exclude all foreground LiDAR points. Here, we have obtained the first frame’s background LiDAR points. Taking one LiDAR point $X \in \mathbb{R}^3$ as an example, we project it onto the remaining $T - 1$ frames using vehicle poses. Formally, the projected point at the time t is:

$$X_t = W_t^{-1} \cdot W_1 \cdot X \quad (6)$$

Here, W_t represents the transformation from the ego vehicle to the world coordinate system at the time t .

4.2 Annotations on Vehicles

In contrast to the background, the vehicle exhibits its own distinctive motion. To account for this, we follow [27] to introduce 3D bounding boxes from 3D object tracking to provide the transformation B_t from the world to the box coordinate system at the time t . We use the 3D bounding boxes to filter out all vehicle LiDAR points. Taking one LiDAR point $X \in \mathbb{R}^3$ as an example, the projected point at the time t is:

$$X_t = W_t^{-1} \cdot B_t^{-1} \cdot B_1 \cdot W_1 \cdot X \quad (7)$$

4.3 Annotations on Pedestrians

The intricacy and non-rigidity of pedestrian movement determine their annotation difficulties, as evidenced by its absence in existing SFE datasets. We employ binocular video to address this challenge indirectly. Firstly, we prepare a segment of T -frames of rectified binocular video.

Then, we employ a semi-automated annotation pipeline to efficiently and accurately label the 2D trajectories of interested points in the left and right view videos.

Labeling the interested point We develop a bespoke annotation software and label the 2D coordinates x_1^l of the interested points within the left image of the first frame.

Computing the coarse left trajectory We utilize Cotracker [19] to compute x_1^l ’s coarse 2D trajectory in the left-view video. Maintaining the first frame’s coordinates, we obtain the trajectory $S^l = \{x_1^l, \dots, x_T^l\}$.

Computing the coarse right trajectory We employ LEAStereo [28] to compute the disparities $\{c_1, \dots, c_T\}$ of the interested point frame by frame. Combining the disparities and S^l , we derive the coarse right trajectory $S^r = \{x_1^r, \dots, x_T^r\}$.

Manual refinement phase The left and right coarse trajectories will be displayed in the annotation software, where the human annotators will correct any low-quality annotations.

Finally, we combine the refined left trajectory with the disparity sequence to construct the 3D trajectory. The depth at frame t is:

$$d_t = f_x \cdot b / c_t \quad (8)$$

Here b is the binocular baseline length. Figure 2 illustrates an example of producing LSFE annotations for pedestrian samples.

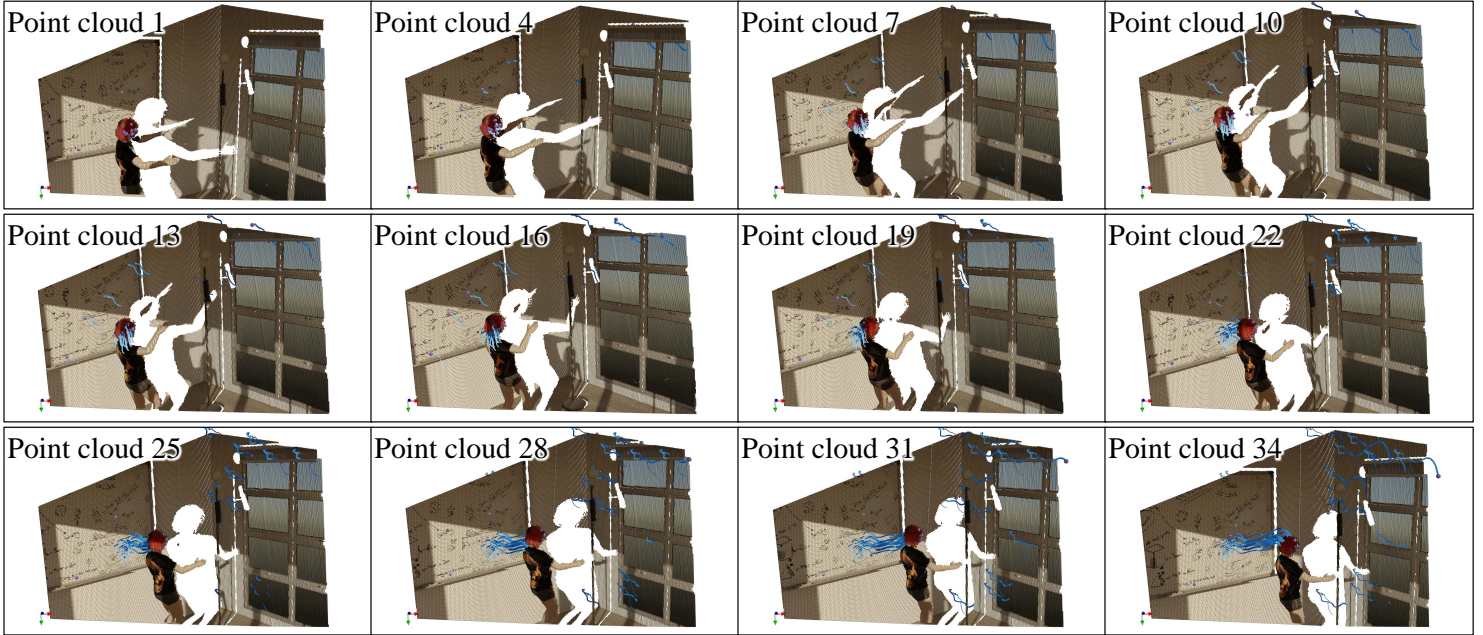


Fig. 3: Visualizations of our SceneTracker’s estimation results on the LSFODyssey test dataset. The predicted 3D trajectories are depicted in blue on their corresponding point clouds.

5 EXPERIMENTS

5.1 Datasets and Experimental Setup

5.1.1 Datasets

LSFODyssey Unlike optical and scene flow tasks, LSFE lacks a dedicated dataset. We reorganize the PointOdyssey [20] dataset initially proposed for the TAP task. PointOdyssey is a large-scale synthetic dataset and data generation framework for the training and evaluation of TAP methods. Fortunately, it can selectively output the depth maps corresponding to RGB images and trajectories in the depth dimension, providing opportunities for training and evaluating LSFE methods. We construct an augmented dataset called LSFODyssey based on the current PointOdyssey [20] dataset to tailor to the LSFE task and reduce dataset reading time to expedite training. The LSFODyssey dataset comprises 127,437 training data samples acquired through data augmentation techniques such as random flipping, spatial transformations, and color transformations. Each sample includes a 24-frame 3D video along with 3D trajectories of 256 query points. Furthermore, we ensure that all query points are non-occluded in at least the first four frames and a total of 12 frames in the video. Besides, we evenly partition 90 testing data samples without applying data augmentation techniques. Each sample consists of 40 frames and includes 256 query points. The entire LSFODyssey dataset is approximately 240GB in size.

LSFDriving Following the Section 4, we construct the first real-world evaluation dataset LSFDriving for the LSFE field. We obtained RGB videos and annotations for backgrounds and vehicles from the Waymo [26] dataset. Due to the absence of binocular cameras in Waymo, we apply depth completion methods to generate dense depth sequences. Specifically, we interpolate the nearest neighbors. It is worth noting that we utilize completed depth maps to establish occlusion relationships, thereby providing valid masks for evaluation. Meanwhile, we acquired RGB videos for pedestrians from the KITTI [29] raw data collection. We utilize LEAStereo [28] to provide dense depth sequences and the proposed semi-automated annotation pipeline to provide

annotations. We do not offer annotations for left-view occluded and binocular non-co-visible regions. Ultimately, each category comprises 60 testing data samples consisting of 40 frames. There are 5 query points for each background and vehicle sample. We annotate 1-5 challenging non-rigid motion points in every pedestrian sample, such as joint and garment points.

5.1.2 Evaluation Metrics

It is common to use metrics the average 2D position accuracy δ_{2D}^{avg} , the median 2D trajectory error MAE_{2D} , and the 2D “Survival” rate $Survival_{2D}$ when evaluating the predicted 3D trajectory’s 2D performance. Here, δ_{2D}^{avg} quantifies the proportion of trajectory points falling within a specified distance threshold from the ground truth, averaged across thresholds $\{1, 2, 4, 8, 16\}$, specified within a normalized resolution of 256×256 . $Survival_{2D}^{16}$ evaluates the percentage of frames in which the initial successful tracking occurs; tracking is deemed unsuccessful if the error exceeds 16 pixels in the normalized 256×256 resolution.

When evaluating the 3D performance of trajectories, we employ the following configuration. We utilize δ_{3D}^x s and their average value δ_{3D}^{avg} to measure the percentage of trajectory points within a threshold distance $x \in \{0.10, 0.20, 0.40, 0.80\}m$ to ground truth. We use median 3D trajectory error MAE_{3D} and 3D end-point error EPE_{3D} to measure the distance between the estimated trajectories and ground truth trajectories. Similarly, we utilize metric $Survival_{3D}^{0.50}$, with a failure threshold set at $0.50m$.

5.1.3 Implementation Details

We use PyTorch to implement our method. We use the AdamW [30] as an optimizer and the One-cycle [31] as the learning rate adjustment strategy. We set $S = 16$, $s = 8$, $l = 4$, and $r = 3$. We evaluate our method after 4 FIM iterations, *i.e.*, $n = 4$, and we set $M = 6$ for the Transformer Cell network. We use the NVIDIA 3090 GPU for training and inference.

5.1.4 Training Processes

Our training includes a training process named Odyssey. In the Odyssey training process, we train the model on the LSFODyssey

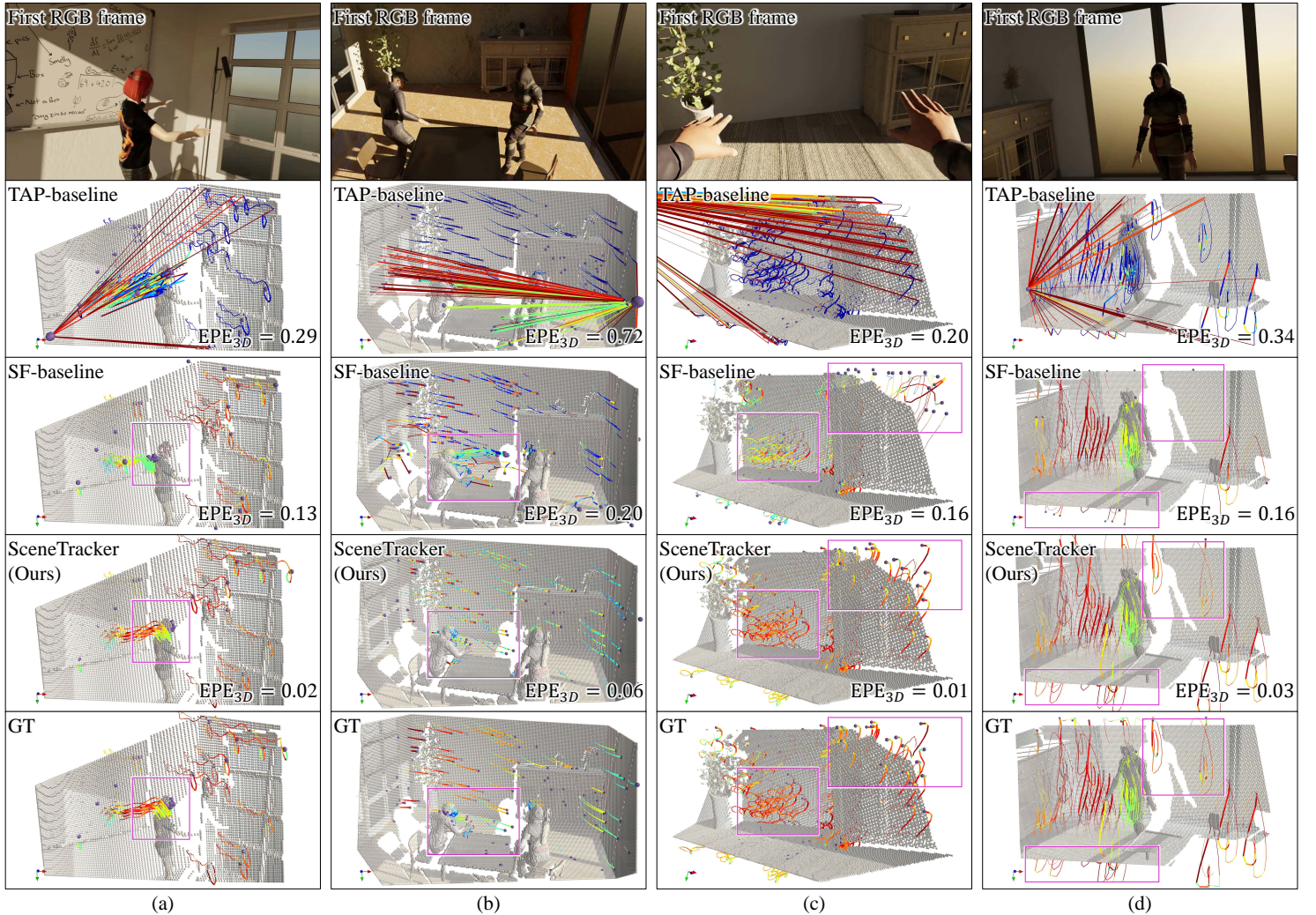


Fig. 4: Qualitative results of the TAP baseline, the SF baseline, and our SceneTracker on the LSFODyssey test dataset. We visualize the trajectory estimates and ground truth of the final frame’s point cloud. The trajectories are colored using a jet colormap. The solid-box marked regions represent areas where the SF baseline exhibits significant errors due to occlusion or exceeding boundaries.

dataset from scratch. Each data sample learns 24 time frames and 256 query points. The input resolution is 384×512 . The batch size is 8. The learning rate is 2×10^{-4} , and the number of training steps is 200K.

5.2 Visualizations of Results

Following the Odyssey training process, we visualize the estimation results of SceneTracker on the LSFODyssey test dataset, as shown in Fig. 3. We present the 12 frames of point clouds from the 40-frame test data sample at equal intervals. The predicted 3D trajectories are depicted in blue on their corresponding point clouds. From Fig. 3, we can see that our method can consistently deliver smooth, continuous, and precise estimation results in the face of the complex motions of the camera and dynamic objects in the scene.

5.3 Comparisons with the SF baseline

We follow RAFT [14] to design a straightforward scene flow baseline named the SF baseline. Since original scene flow methods can only address trajectory prediction problems between two frames, we adopt a chaining approach to handle long videos. Precisely, after calculating the scene flow between the first and

TABLE 1: Quantitative results on the 2D metrics within the LSFODyssey test dataset. All data come from the Odyssey training process.

Method	$\delta_{2D}^{avg} \uparrow$	Survival $_{2D}^{16} \uparrow$	MAE $_{2D} \downarrow$
SF baseline	75.11	92.81	4.90
SceneTracker (Ours)	85.07	96.71	2.01

second frames, we determine the uv coordinates corresponding to the predicted position of the second frame and index the depth of the second frame to obtain the query point coordinates from the second frame to the third frame, and so on for subsequent frames.

We also train the SF baseline on the LSFODyssey dataset from scratch to ensure equity. We use the same training settings as the SceneTracker’s Odyssey training process. After training, we compare our SceneTracker with the SF baseline on the LSFODyssey test dataset. The results are shown in Fig. 4, Table 1 and Table 2.

We can see from Table 1 and Table 2 that our method significantly outperforms the SF baseline across all dataset metrics, both in 2D and 3D metrics. Especially on MAE $_{2D}$ and MAE $_{3D}$,

TABLE 2: Quantitative results on the 3D metrics within the LSFODyssey test dataset. All data come from the Odyssey training process.

Method	$\delta_{3D}^{0.10} \uparrow$	$\delta_{3D}^{0.20} \uparrow$	$\delta_{3D}^{0.40} \uparrow$	$\delta_{3D}^{0.80} \uparrow$	$\delta_{3D}^{avg} \uparrow$	Survival $_{3D}^{0.50} \uparrow$	MAE $_{3D} \downarrow$	EPE $_{3D} \downarrow$
TAP baseline	57.52	67.72	74.45	81.24	70.23	55.76	0.388	0.573
SF baseline	71.78	84.40	92.67	97.33	86.55	93.91	0.123	0.132
SceneTracker (Ours)	88.70	95.57	98.08	99.27	95.41	98.09	0.052	0.058

TABLE 3: The evaluation results of SceneTracker on the LSFDriving dataset after the Odyssey training process, where only points with depth $< 35m$ are considered for evaluation.

Experiment	Variations	vehicle			background			person		
		$\delta_{2D}^{avg} \uparrow$	$\delta_{3D}^{avg} \uparrow$	EPE $_{3D} \downarrow$	$\delta_{2D}^{avg} \uparrow$	$\delta_{3D}^{avg} \uparrow$	EPE $_{3D} \downarrow$	$\delta_{2D}^{avg} \uparrow$	$\delta_{3D}^{avg} \uparrow$	EPE $_{3D} \downarrow$
SF baseline	-	77.51	39.61	1.262	81.15	55.13	0.717	40.74	23.01	1.523
SceneTracker +“Single” inference mode	-	73.98	36.45	1.595	73.69	38.36	1.548	43.64	15.48	2.902
	local	85.16	66.40	0.331	86.07	58.53	0.605	57.13	35.28	0.737
	global	81.46	55.61	0.409	84.44	58.74	0.596	56.18	39.36	0.603
	local & global	85.50	65.75	0.287	87.13	60.88	0.472	57.79	37.98	0.707
SceneTracker +“All” inference mode	-	81.45	50.71	1.011	81.56	56.56	0.579	43.34	14.87	2.890
	global	83.42	67.54	0.252	83.70	63.87	0.351	59.00	41.32	0.486

SceneTracker achieves error reductions of 59.0% and 57.7%, respectively. In contrast to the SFE approach, our method employs identical query point features as initial templates tracked for each window, avoiding query point drift. This strategy effectively addresses occlusion and out-of-boundary effects, further substantiated in Fig. 4’s solid-box marked regions. The results fully demonstrate our method’s superior performance. The experimental findings substantiate the efficacy of our approach in tackling the LSF challenge.

5.4 Comparisons with the TAP baseline

We observe that our estimated 3D trajectories can be projected onto the image plane to form a continuous 2D trajectory, which serves as the output of the TAP task. For this purpose, we construct a TAP baseline based on SceneTracker. Specifically, the TAP baseline first outputs the image plane uv trajectory, then utilizes the uv trajectory to index into the depth map of each frame, and finally transforms the indexed uvd trajectory into the camera coordinate system.

We utilize SceneTracker trained through the Odyssey training process to provide 2D trajectories for the TAP baseline. After training, we compare our SceneTracker with the TAP baseline on the LSFODyssey test dataset. The results are shown in Fig. 4 and Table 2.

We can see from Table 2 that our approach significantly outperforms the TAP baseline on all 3D dataset metrics. Especially on MAE $_{3D}$ and EPE $_{3D}$, SceneTracker achieves error reductions of 86.6% and 89.9%, respectively. At the same time, on Survival $_{3D}^{0.50}$, SceneTracker achieves a 75.9% increase in accuracy. The significant performance gap stems mainly from the TAP baseline’s lack of robustness against depth noise interference and the inability to handle occlusion relationships in 3D space. It is worth noting that LSFODyssey simulates fog and smoke, setting their depths as outliers directly, resulting in a depth map with a substantial amount of noise, posing significant challenges. The TAP baseline, due to its direct indexing from the depth map, is unable to detect and correct erroneous depth data, which is also substantiated in Fig. 4.

The results fully demonstrate that the proposed method excels in spatial relationship handling and noise resistance, highlighting the unique challenges the LSF task poses.

5.5 Results on WWDiving



Fig. 5: Examples of the proposed LSFDriving dataset.

This subsection mainly analyzes the performance of our method on real-world data. TABLE 3 shows the evaluation results of our SceneTracker under different inference modes on the LSFDriving dataset, whose examples are shown in Fig. 5, after the Odyssey training process. We evaluate the three types of points in LSFDriving separately. We test the “Single” and “All” inference modes. In the “Single” inference mode, the network tracks only one query point at a time, while in the “All” inference mode, it tracks all query points simultaneously. Since each sample in LSFDriving only requires tracking up to five points, even tracking all query points simultaneously (“All” inference mode) does not provide the network with rich cross-space context. Therefore, we make the network incorporate additional auxiliary points, such as local points within the vicinity of the target point and global points uniformly distributed across the entire image, to track them together.

It can be seen from Table 3 that adding auxiliary points can significantly enhance the network’s performance, irrespective of the inference mode. Simultaneously, the “All” inference mode

exhibits superior performance across all 3D dataset metrics with auxiliary points. Furthermore, we observe that errors in pedestrian samples are consistently higher than those in background and vehicle samples. This fully showcases the complexity and challenges posed by non-rigid motions.

Overall, our method demonstrates commendable performance in real-world scenes while training solely on synthetic datasets.

5.6 Ablation Studies

TABLE 4: Quantitative results about the template feature updates.

Experiment	$\delta_{3D}^{avg} \uparrow$	Survival $_{3D}^{0.50} \uparrow$	MAE $_{3D} \downarrow$	EPE $_{3D} \downarrow$
No Update	95.27	98.04	0.055	0.061
SceneTracker	95.41	98.09	0.052	0.058

Updates of the template feature We halt the template feature updates to assess the impact of the dynamic cost volume on the network’s performance. The performance degradation induced by the locking of template features in Table 4 elucidates that LSFE necessitates a greater focus on addressing the variations in feature distribution brought about by long sequences in comparison to SFE.

TABLE 5: Quantitative results about the sliding window size.

Window Size	$\delta_{3D}^{avg} \uparrow$	Survival $_{3D}^{0.50} \uparrow$	MAE $_{3D} \downarrow$	EPE $_{3D} \downarrow$
8	93.32	97.77	0.070	0.075
12	94.88	98.04	0.058	0.062
16	95.41	98.09	0.052	0.058
20	85.81	97.23	0.099	0.116
24	81.47	95.41	0.144	0.174

Inference sliding window size In Table 5, we inspect how the inference sliding window size affects model performance. We find that an inference window size $S = 16$ achieves optimal performance across all dataset metrics.

6 CONCLUSION

In summary, we propose a new task, *i.e.*, long-term scene flow estimation, to capture the fine-grained and long-term 3D motion better. To effectively tackle this issue, we introduce a novel approach named SceneTracker. With detailed experiments, SceneTracker shows superior capabilities in handling 3D spatial occlusion and depth noise interference, highly tailored to the LSFE task’s needs. Finally, we build the first real-world evaluation dataset, LSFDiving, further substantiating SceneTracker’s commendable generalization capacity.

Through this work, we further prove the feasibility of simultaneously capturing fine-grained and long-term 3D motion, and the LSFE task is poised to become a promising direction for future research.

REFERENCES

- [1] T. Yin, X. Zhou, and P. Krahenbuhl, “Center-based 3d object detection and tracking,” in *CVPR*. IEEE, 2021, pp. 11 784–11 793.
- [2] Z. Pang, Z. Li, and N. Wang, “Simpletrack: Understanding and rethinking 3d multi-object tracking,” in *ECCV*. Springer, 2022, pp. 680–696.
- [3] X. Chen, S. Shi, C. Zhang, B. Zhu, Q. Wang, K. C. Cheung, S. See, and H. Li, “Trajectoryformer: 3d object tracking transformer with predictive trajectory hypotheses,” in *ICCV*. IEEE, 2023, pp. 18 527–18 536.
- [4] X. Liu, C. R. Qi, and L. J. Guibas, “FlowNet3d: Learning scene flow in 3d point clouds,” in *CVPR*, 2019, pp. 529–537.
- [5] C. R. Qi, L. Yi, H. Su, and L. J. Guibas, “Pointnet++: Deep hierarchical feature learning on point sets in a metric space,” *Advances in neural information processing systems*, vol. 30, 2017.
- [6] H. Liu, T. Lu, Y. Xu, J. Liu, W. Li, and L. Chen, “Camliflow: bidirectional camera-lidar fusion for joint optical flow and scene flow estimation,” in *CVPR*, 2022, pp. 5791–5801.
- [7] G. Yang and D. Ramanan, “Upgrading optical flow to 3d scene flow through optical expansion,” in *CVPR*, 2020, pp. 1334–1343.
- [8] Z. Teed and J. Deng, “Raft-3d: Scene flow using rigid-motion embeddings,” in *CVPR*, 2021, pp. 8375–8384.
- [9] G. Yang and D. Ramanan, “Learning to segment rigid motions from two frames,” in *CVPR*, 2021, pp. 1266–1275.
- [10] A. Dosovitskiy, P. Fischer, E. Ilg, P. Hausser, C. Hazirbas, V. Golkov, P. Van Der Smagt, D. Cremers, and T. Brox, “FlowNet: Learning optical flow with convolutional networks,” in *ICCV*. IEEE, 2015, pp. 2758–2766.
- [11] D. Sun, X. Yang, M.-Y. Liu, and J. Kautz, “Pwc-net: Cnns for optical flow using pyramid, warping, and cost volume,” in *CVPR*. IEEE, 2018, pp. 8934–8943.
- [12] T.-W. Hui, X. Tang, and C. C. Loy, “Liteflownet: A lightweight convolutional neural network for optical flow estimation,” in *CVPR*. IEEE, 2018, pp. 8981–8989.
- [13] H. Xu, J. Zhang, J. Cai, H. Rezatofighi, F. Yu, D. Tao, and A. Geiger, “Unifying flow, stereo and depth estimation,” *IEEE Transactions on Pattern Analysis and Machine Intelligence (TPAMI)*, 2023.
- [14] Z. Teed and J. Deng, “Raft: Recurrent all-pairs field transforms for optical flow,” in *ECCV*. Springer, 2020, pp. 402–419.
- [15] S. Jiang, D. Campbell, Y. Lu, H. Li, and R. Hartley, “Learning to estimate hidden motions with global motion aggregation,” in *ICCV*. IEEE, 2021, pp. 9772–9781.
- [16] B. Wang, Y. Zhang, J. Li, Y. Yu, Z. Sun, L. Liu, and D. Hu, “Splatflow: Learning multi-frame optical flow via splatting,” *International Journal of Computer Vision*, pp. 1–23, 2024.
- [17] C. Doersch, A. Gupta, L. Markeeva, A. Recasens, L. Smaira, Y. Aytar, J. Carreira, A. Zisserman, and Y. Yang, “Tap-vid: A benchmark for tracking any point in a video,” *Advances in Neural Information Processing Systems*, vol. 35, pp. 13 610–13 626, 2022.
- [18] M. Neoral, J. Šerých, and J. Matas, “Mft: Long-term tracking of every pixel,” in *WACV*, 2024, pp. 6837–6847.
- [19] N. Karaev, I. Rocco, B. Graham, N. Neverova, A. Vedaldi, and C. Rupprecht, “Cotracker: It is better to track together,” *arXiv preprint arXiv:2307.07635*, 2023.
- [20] Y. Zheng, A. W. Harley, B. Shen, G. Wetzstein, and L. J. Guibas, “Pointodyessey: A large-scale synthetic dataset for long-term point tracking,” in *ICCV*. IEEE, 2023, pp. 19 855–19 865.
- [21] A. W. Harley, Z. Fang, and K. Fragkiadaki, “Particle video revisited: Tracking through occlusions using point trajectories,” in *ECCV*. Springer, 2022, pp. 59–75.
- [22] B. Kerbl, G. Kopanas, T. Leimkühler, and G. Drettakis, “3d gaussian splatting for real-time radiance field rendering,” *ACM Transactions on Graphics*, vol. 42, no. 4, pp. 1–14, 2023.
- [23] J. Luiten, G. Kopanas, B. Leibe, and D. Ramanan, “Dynamic 3d gaussians: Tracking by persistent dynamic view synthesis,” *arXiv preprint arXiv:2308.09713*, 2023.
- [24] G. Wu, T. Yi, J. Fang, L. Xie, X. Zhang, W. Wei, W. Liu, Q. Tian, and X. Wang, “4d gaussian splatting for real-time dynamic scene rendering,” *arXiv preprint arXiv:2310.08528*, 2023.
- [25] M. Menze and A. Geiger, “Object scene flow for autonomous vehicles,” in *CVPR*. IEEE, 2015, pp. 3061–3070.
- [26] P. Sun, H. Kretzschmar, X. Dotiwalla, A. Chouard, V. Patnaik, P. Tsui, J. Guo, Y. Zhou, Y. Chai, B. Caine *et al.*, “Scalability in perception for autonomous driving: Waymo open dataset,” in *CVPR*, 2020, pp. 2446–2454.
- [27] A. Balasingam, J. Chandler, C. Li, Z. Zhang, and H. Balakrishnan, “Drivetrack: A benchmark for long-range point tracking in real-world videos,” *arXiv preprint arXiv:2312.09523*, 2023.
- [28] X. Cheng, Y. Zhong, M. Harandi, Y. Dai, X. Chang, H. Li, T. Drummond, and Z. Ge, “Hierarchical neural architecture search for deep stereo matching,” *Advances in Neural Information Processing Systems*, vol. 33, pp. 22 158–22 169, 2020.
- [29] A. Geiger, P. Lenz, and R. Urtasun, “Are we ready for autonomous driving? the kitti vision benchmark suite,” in *CVPR*. IEEE, 2012, pp. 3354–3361.
- [30] I. Loshchilov and F. Hutter, “Decoupled weight decay regularization,” *arXiv preprint arXiv:1711.05101*, 2017.
- [31] L. N. Smith and N. Topin, “Super-convergence: Very fast training of neural networks using large learning rates,” in *Artificial intelligence and machine learning for multi-domain operations applications*, vol. 11006. SPIE, 2019, pp. 369–386.